Journal of Industrial Aerodynamics, 1(1975) 177—199
Elsevier Scientific Publishing Company, Amsterdam — Printed in The Netherlands

A STUDY OF WIND PRESSURES ON A SINGLE-FAMILY DWELLING IN MODEL AND FULL SCALE*

RICHARD D. MARSHALL
National Bureau of Standards, Washington, D.C. 20234 (USA)

(Received January 21, 1975)

Summary

Wind pressures measured on a single-family dwelling are compared with results obtained from a 1:50 scale model placed in a turbulent boundary layer. It is shown that the fluctuating components of surface pressures far exceed the mean or steady pressures and are well-correlated over sizeable roof areas. The consistently low fluctuating pressure coefficients obtained from the wind tunnel model are attributed to improper simulation of the lower portion of the atmospheric boundary layer. Comparisons between actual loads and specified design loads suggest that certain current provisions are marginal for tributary areas and excessive for localized areas such as ridges, eaves and corners. A procedure for expressing loads on both localized and extended roof areas in terms of mean pressure coefficients and a peak factor is described.

1. Introduction

Research over the past ten years into the effects of wind on buildings and other structures is significantly influencing design philosophy and practice. This is evidenced by recent major revisions of building codes and standards, both here in the United States and abroad. Perhaps the most significant improvement has been the recognition of wind loading as a stochastic process and the formulation of design criteria based upon acceptable levels of risk. Other improvements include provisions for various classes or categories of terrain roughness and the wind tunnel simulation of the atmospheric boundary layer when measuring pressure coefficients and dynamic response factors.

In spite of these important advances, considerable work remains to be done. This is particularly true of existing criteria covering the design of low-rise buildings which have not benefited from this research in the same proportion as tall structures. It is interesting to note that pressure coefficients in current use are based, to a great extent, on wind tunnel studies carried out in uniform flows of low turbulence, using instrumentation capable of measuring only

*Paper presented at the Symposium on Full-Scale Measurements of Wind Effects on Tall Buildings and Other Structures, University of Western Ontario, 23—29 June 1974.

mean pressures. It is obvious, therefore, that a major effort must be made to improve wind tunnel modeling of low-rise structures. Once this is accomplished, pressure coefficients and response factors can be determined in an efficient and systematic manner.

Prior to this, however, the validity of modeling techniques must be established by comparing test results with representative measurements obtained from full-scale buildings. The investigation described in the following sections is an attempt to provide a preliminary comparison between model and full-scale test results for a single-family dwelling.

2. The test site

The site selected for this study is located at Malmstrom Air Force Base, Montana, directly to the east of the city of Great Falls. The region is noted for its "Chinook" winds which regularly blow out of the southwest during the winter months. The terrain surrounding the test site is markedly flat and free of significant obstructions. Although the mean hourly speeds for the area are quite high (6—8 m/s), extreme winds seldom exceed 30 m/s.

The building investigated is a single-family dwelling, one of four quite similar units located in an area having a clear wind exposure extending from the west clockwise around to the south. A cluster of two-story housing units is located approximately 100 m southwest of the test site and extends in that direction for approximately 550 m (see Figs. 1 and 2). The test building and adjacent structures are shown in Fig. 2. The test building has basic plan dimensions of 6.8 × 23 m with a 5 × 5.8-m wing (Fig. 3). The roof pitch is is 11.5° and the eaves overhang is 0.8 m.

3. Full-scale test procedure

Surface pressures were measured at 9 points on the roof (P1—P9) and at one point under the eaves (P10) as indicated in Fig. 3. The internal pressure (P12) was measured in the garage which is located directly under the instrumented portion of the roof. An additional pressure tap (P11) was installed under the eaves in the wind tunnel model. To avoid penetrating the roof membrane with conventional pressure taps and, at the same time, to accurately measure pressures over the roof surface, the pressure transducers were mounted under low-profile housings having a height of 3.6 cm and a diameter of 61 cm. All transducers were referenced to a vane-mounted pitot static tube located 2.9 m above the ridge line, *i.e.*, 6.1 m above ground level.

Wind speed and direction were obtained with a propeller-vane anemometer located 6.6 m above ground level. A standard National Weather Service three-cup anemometer was used to trigger the data acquisition system when wind speeds exceeded a preset level. Positions of the pitot static probe and anemometers are shown in Fig. 3.

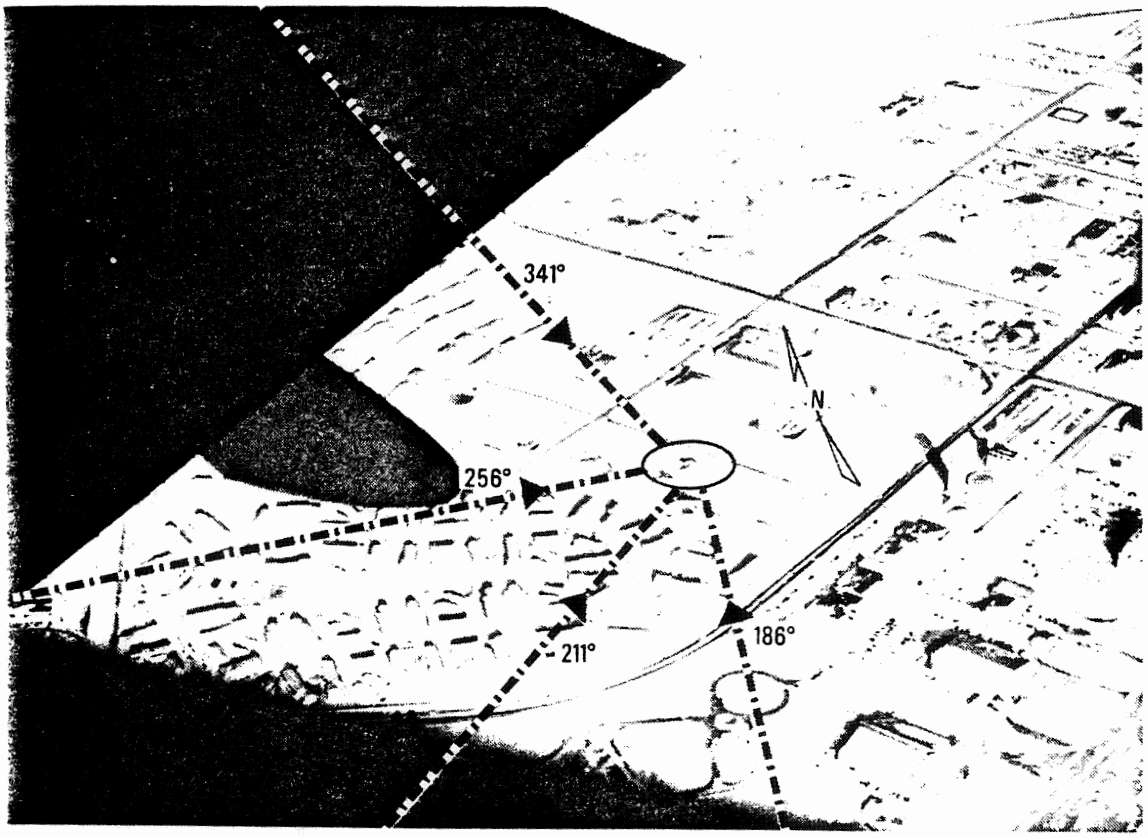

Fig. 1. Aerial view of the test site.

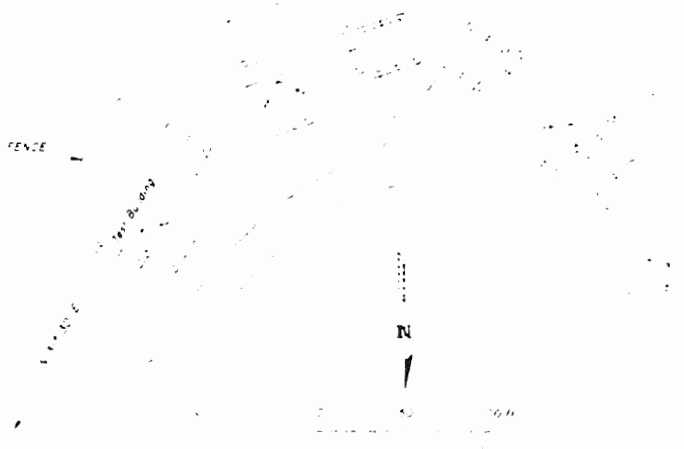

Fig. 2. Test site layout.

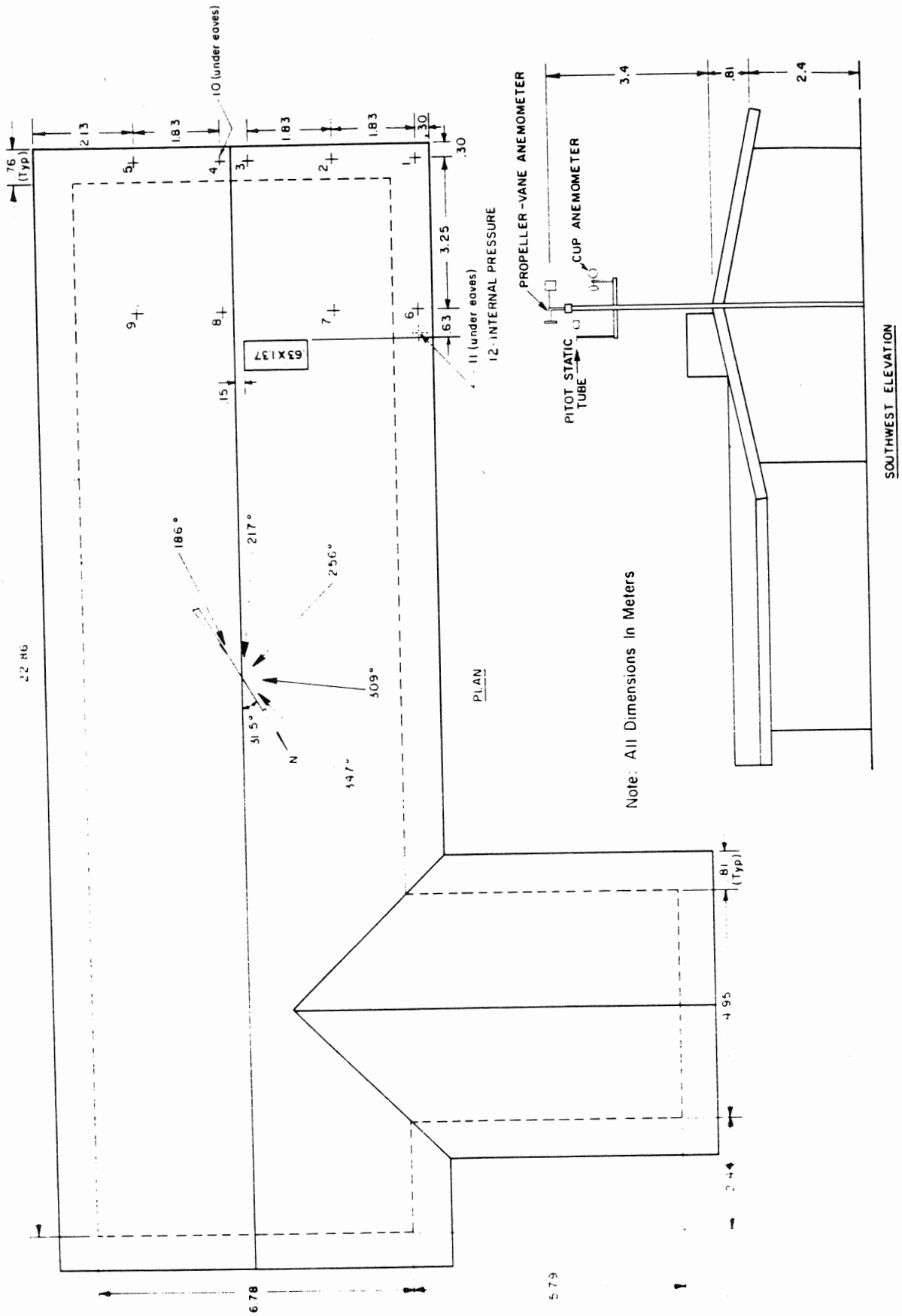

Fig. 3. Plan and elevation of the test building.

A 14-channel analog tape recorder was used to acquire data. In addition to the eleven pressure signals, and wind speed and direction, a time code was recorded to identify the data runs or records. Normal operating procedure was to set the system threshold at 18 m/s and record for 15 min. The system would then enter a 1-h hold period before checking the wind speed against the preset value. While this procedure resulted in a number of redundant records, it did provide data corresponding to peak winds in winter storms passing through the region. These storms generally had a duration of from one to three days. Barometric pressure, temperature and other weather data were obtained from hourly observations made by the 3rd Weather Wing, USAF.

4. Wind tunnel test procedure

In order to increase the value of the full-scale test results, aid in their interpretation and explore the feasibility of modeling the natural wind at an unconventional scale, a series of wind tunnel tests were conducted during the course of the study using a model scale of 1:50.

The tunnel used for these tests is one of several operated by Colorado State University and has a 1.83-m-square by 12-m-long working section. To simulate the natural wind, a thick shear layer was established by use of a row of spires and a sawtooth fence installed at the working section entrance. In addition,

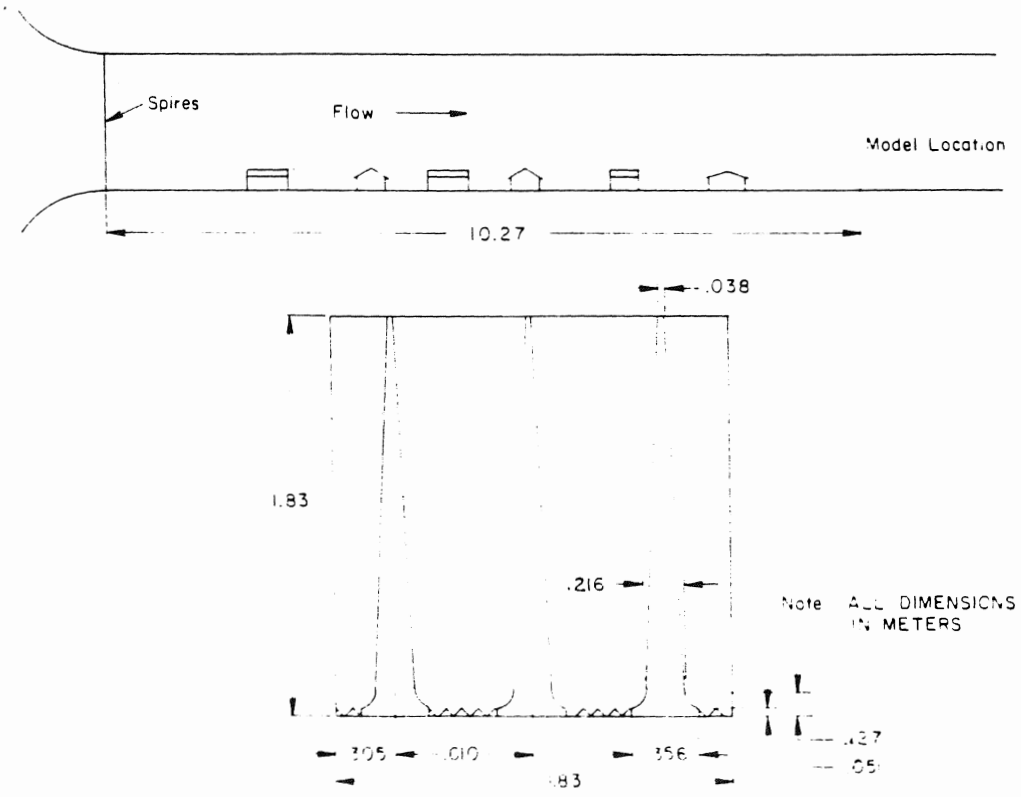

Fig. 4. Wind tunnel layout.

all adjacent and upwind structures were modeled in the tunnel. This approach has been described by Melbourne [1] and Standen [2] and when compared with results obtained using surface roughness elements alone, it substantially increased the growth rate of the boundary layer and increased the scale of turbulence at the position of the model, 10.3 m downstream from the spires. Spire details and position of the model are shown in Fig. 4.

Pressures were measured with the same transducers and recording system used for the full-scale study. The orifice-tube combinations exhibited a satisfactory frequency response out to 100 Hz. All pressure measurements were referenced to a pitot static tube located 1.22 m above the tunnel floor, directly over the building model. Wind speed records and static and dynamic pressures were obtained by means of a hot-wire anemometer and pitot tube located in the same relative positions as the instruments in the full-scale study. In addition, mean velocity profiles were obtained at the position of the model for each of the four wind directions studied.

5. Data reduction and analysis

Analog tapes containing full-scale and wind tunnel data were processed using the data system described in ref. [3]. The usual procedure was to plot the full-scale wind speed and direction records on a stripchart recorder and then to select those records exhibiting a satisfactory degree of stationarity for detailed analysis. Analog to digital conversion was accomplished at a rate of sixteen samples per second with a total of 12,000 samples per record or a digital record length of 750 seconds. By using a reduced playback speed, it was possible to digitize the wind tunnel data at the same effective rate and account for the 50:1 change in time scale. Thus the time and frequency scales were assumed to be identical in the subsequent data analysis. With the exception of the hot-wire records, all records were obtained from transducers exhibiting linear characteristics.

A series of computer programs have been developed at the NBS for the analysis of random data. These include PROGRAM 2 which formats sequential channel samples into sequential samples for a given channel; CORREL which performs low-pass filtering and contains options for computing the mean, r.m.s., auto- and cross-correlation, spectral density and coherence functions; PDF which computes probability densities and tabulates peak values and associated zero-crossing rates; and SUMP which generates a new data series based on the area integration of surface pressures. In addition, subroutines exist for linearizing hot-wire records and correcting fixed-direction-propeller anemometer records for departures from the cosine law.

In the study reported herein, no attempt was made to remove trends from the data series prior to analysis, the records being visually screened before conversion. However, even with this screening, there were certain records processed which indicated significant trends as reflected by their segmental means and auto-correlation functions. Most steps in the analysis were preceded

by low-pass filtering, each four successive samples being averaged and resulting in a record size of 3000 samples. Auto-correlations were calculated for 200 lags, followed by 0.02 Hz fixed-bandwidth spectral analysis.

6. Measurement results and discussion

Field measurements at the Montana test site were obtained over a 5-month period during 1971—72, yielding approximately 15 hours of recordings (60 records) under strong wind conditions. Four different wind directions were selected for subsequent wind tunnel simulation on the basis of differing obstructions over the wind fetch. Due to demands placed on test equipment, only a preliminary analysis of the field data was available at the time the wind tunnel studies were conducted. This proved to be unfortunate in that a better simulation of the natural wind could have been achieved with slight additional effort.

In the following sections, run numbers with three digits designate full-scale data. Wind azimuth angles (β) are measured clockwise from north. Five typical full-scale records were selected for detailed analysis and comparison with the wind tunnel test results.

6.1 Simulation of the atmospheric boundary layer

Because of the model scale used in this study and the physical size of the wind tunnel facility, a simulation of only the lower 30 m of the atmospheric

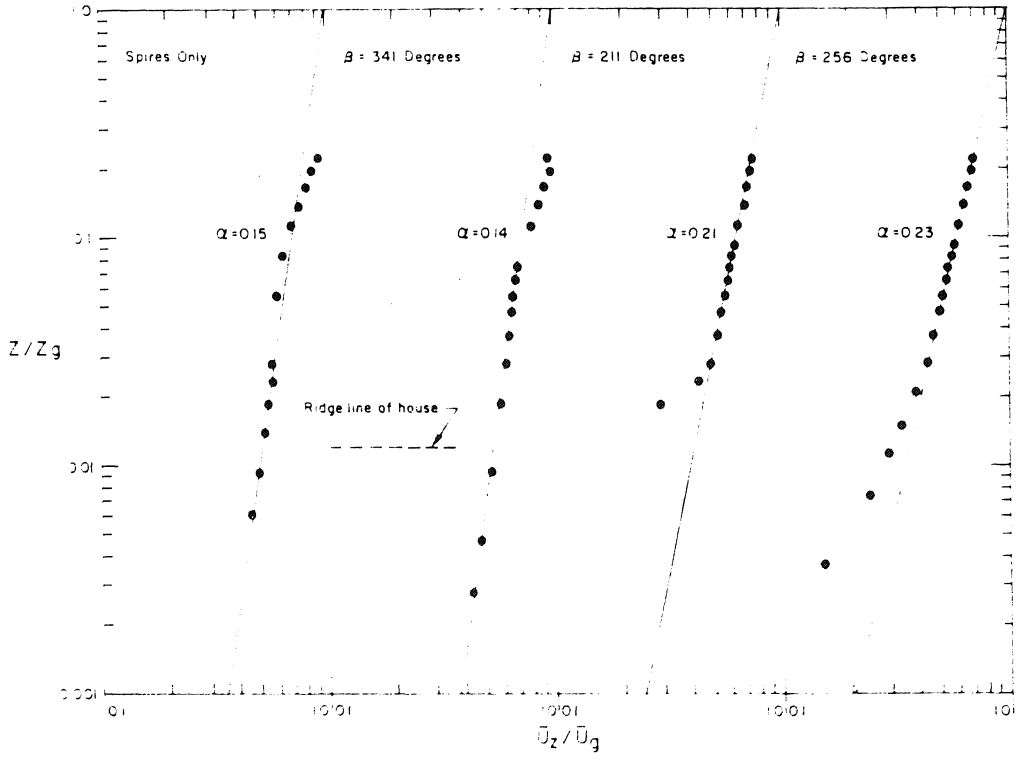

Fig. 5. Mean velocity profiles — power law representation.

boundary layer was attempted. Restrictions placed on the use of the field test site did not allow the installation of a meteorological tower of sufficient height to establish characteristics of the atmospheric boundary layer over this range. Field measurements of wind speed were thus limited to one point, 6.6 m above ground level. As will be discussed later, this necessitated corrections to the mean reference speeds and pressures during the data analysis.

Typical mean velocity profiles measured at the position occupied by the model (10.3 m downstream) are shown in Fig. 5 as a power law representation. In plotting these profiles, it was assumed that the actual scale of the shear flow was 1:50 and that the thickness of the atmospheric boundary layer was 275 m. The first profile corresponds to the case of only the spires and sawtooth fence installed and exhibits a satisfactory velocity distribution only up to a full-scale height of approximately 10 m. The second profile corresponds to an azimuth angle of $\beta = 341^\circ$, the direction having the least number of structures upwind. Although the profile agrees well with the power law up to approximately 27 m, there is a substantial departure above this height. Only for azimuth angles of 186, 211 and 256° did the mean velocity profiles correspond to the power law above 30 m. The departure of the profile for $\beta = 211^\circ$ from the power law for $Z/Z_G < 0.025$ is due to the neighboring house directly upwind.

While the exponents obtained from the plots in Fig. 5 are in good agreement with recommended values for terrain typical of the test site, there is nothing to suggest that the scale ratio is, in fact, 1:50. The profiles for β =

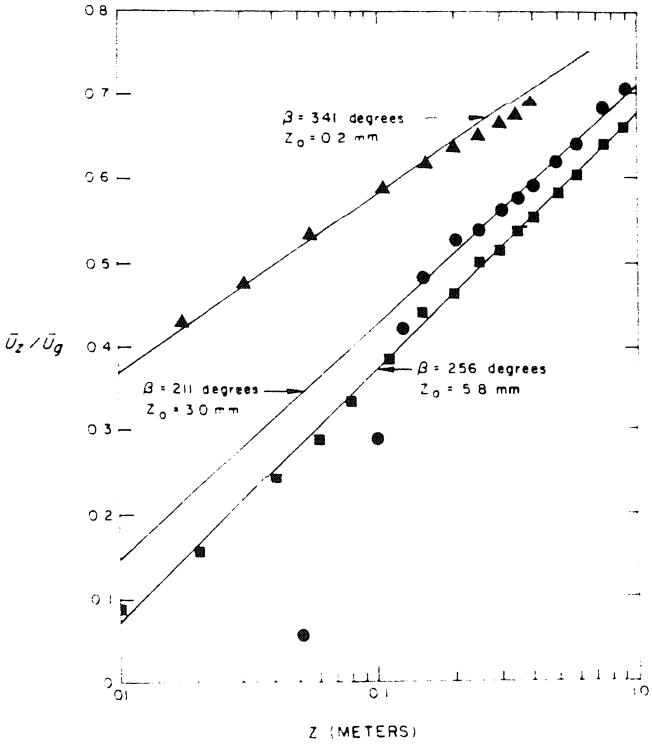

Fig. 6. Mean velocity profiles — log law representation.

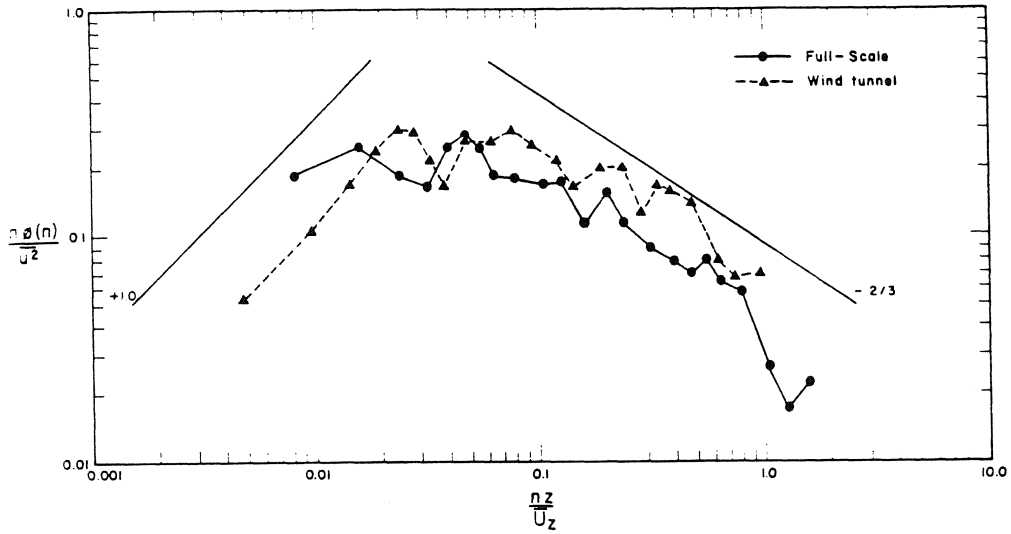

Fig. 7. Velocity spectra (Run Nos. 311 and 22).

211, 256 and 341° are plotted as a log law in Fig. 6. The corresponding roughness heights (Z_o), were found to be 0.30, 0.58 and 0.02 cm. Helliwell [4] determined a value of 8 cm for open country at Heathrow and Cardington. This would suggest a scale ratio of from 1:15 to 1:400 for the atmospheric boundary layer simulation. Only the very lowest portion of the profile for $\beta = 341°$ corresponds to the log law and it is suggested that the scale ratios associated with the peaks of the turbulence spectra are more meaningful.

Typical spectral density functions for $\beta = 256°$ (Run Nos. 311 and 22) and $Z = 6.6$ m are plotted on Monin coordinates in Fig. 7. The wavelengths associated with spectral peaks are approximately 3.3 and 265 m for model

TABLE 1

Flow properties

Run No.*	Direction (degrees)	$\bar{U}_R$ (m/s)	$\sqrt{\overline{u^2}}$ (m/s)	I (%)	Maximum peak (m/s)	Zero crossing rate (Hz)	$\bar{U}_{10}$ (m/s)
207	186	11.37	3.38	30	19.93	0.267	12.07
21	186	11.89	2.54	21	—	—	12.62
310	217	7.77	2.93	38	18.41	0.158	9.14
23	211	13.17	4.08	31	—	—	15.51
24	211	18.71	1.10	6	—	—	18.78
311	256	8.38	2.62	31	16.25	0.169	8.47
22	256	14.69	2.59	18	—	—	15.06
322	309	9.91	2.35	24	15.64	0.166	10.36
11	341	13.78	1.43	10	—	—	14.14
101	347	9.24	2.50	27	14.81	0.211	9.45

*Run numbers with 3 digits denote full-scale data.

and full-scale respectively, indicating a scale ratio of 1:80 for this wind direction. It is seen that the slopes of the spectra below and above the peaks agree reasonably well with those of the von Karman spectral density function, +1.0 and −2/3, respectively. The scale ratios obtained in this manner for $\beta = 211$ and 341° were found to be 1:90 and 1:60, respectively.

Flow properties for four groups of directions are listed in Table 1. Unfortunately, turbulence measurements were obtained only at $Z = 6.6$ m, these being limited to the longitudinal component. With the exception of $\beta = 211°$, the turbulence intensities measured in the tunnel are approximately 50% of the corresponding full-scale values. Run No. 24 for $\beta = 211°$ was obtained with the spires and upwind models removed from the tunnel, the boundary layer thickness for this case being approximately 0.40 m. Also included in Table 1 are the maximum speeds observed in the full-scale data over a time interval of 750 seconds, the average frequency of occurrence of peak values (commonly referred to as the zero crossing rate), and the mean velocity at $Z = 10$ m. Full-scale values of $\bar{U}_{10}$ are based upon the ratio $\bar{U}_{10}/\bar{U}_R$ which was measured in the wind tunnel.

The use of spires and roughness elements in tunnels with short working sections results in mean velocity profiles that are quite acceptable when compared with either the log law or power law representations. However, it is obvious that the turbulence characteristics are not always in satisfactory agreement with full-scale values.

While the shapes of the spectral density functions agree fairly well with the full-scale functions, both the scale and intensity of turbulence are low. This suggests that the surface roughness elements must be modeled at a distorted scale and that a minimum roughness must be maintained in the tunnel when modeling relatively smooth prototype surface conditions.

6.2 Pressure measurements

It was anticipated, and later confirmed by the wind tunnel tests, that corrections would have to be applied to the full-scale dynamic and static reference pressures due to the close proximity of the anemometer and pressure probe to the test building. The procedure was to determine a static pressure correction coefficient:

$$C_{sp} = \frac{\bar{p}_R - \bar{p}_{10}}{1/2\,\rho\,\bar{U}_R^2}$$

in the tunnel and then to apply this correction as an offset to all full-scale pressure records (see p. 198 for Nomenclature). The dynamic pressure correction coefficient:

$$C_{dp} = \frac{1/2\,\rho\,\bar{U}_{10}{}^2}{1/2\,\rho\,\bar{U}_R{}^2}$$

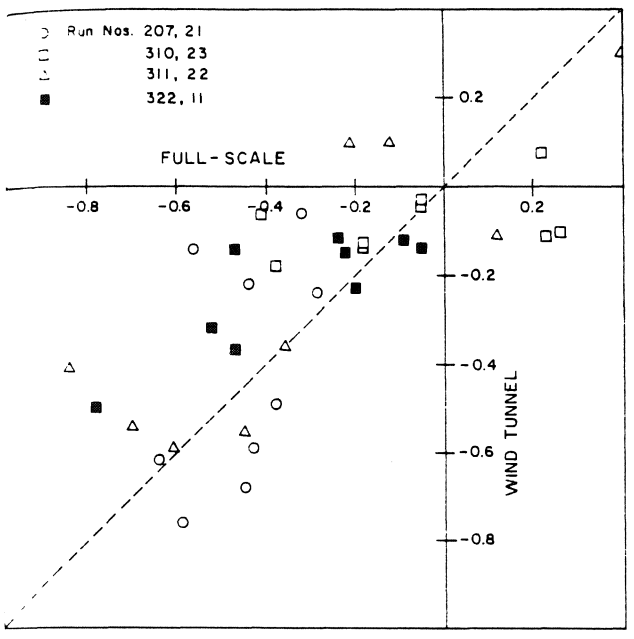

Fig. 8. Mean pressure coefficients.

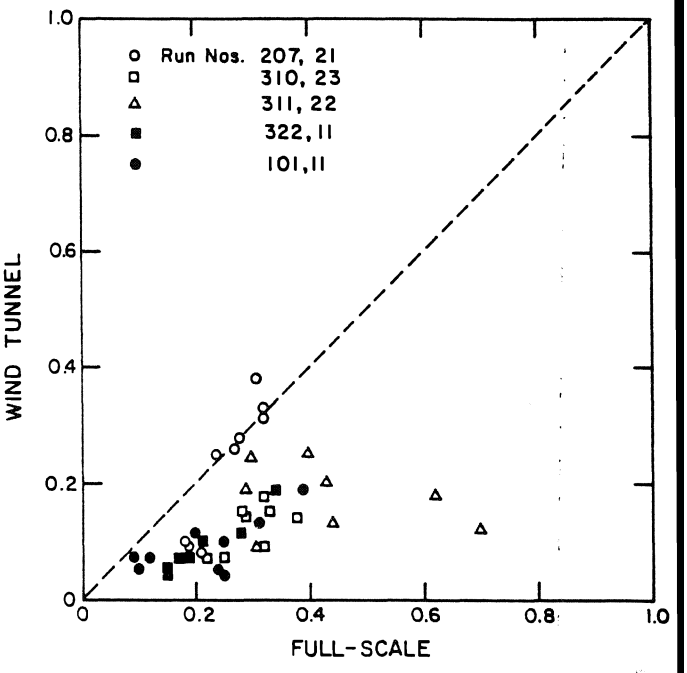

Fig. 9. Fluctuating pressure coefficients.

was applied in a similar manner. Both corrections were direction-dependent and values of C_{sp} and C_{dp} ranged from −0.10 to −0.21 and from 1.02 to 1.39, respectively.

The results of pressure measurements are summarized in Tables 2—5 and are compared graphically in Figs. 8 and 9. The mean pressure coefficient C_p, and the fluctuating pressure coefficient, C_{pf}, correspond to the usual definitions and are referenced to the free-stream dynamic pressure at $Z = 10$ m. The peak factor, g, is defined as the number of standard deviations included in the maximum peak departure from the mean, *i.e.*

$$g = \frac{|p_{\text{max. or min.}} - \bar{p}|}{p_{\text{r.m.s.}}}$$

The zero crossing rates (Table 5) are as previously defined.

The mean pressure coefficients, C_p, plotted in Fig. 8, indicate considerable disagreement between model and full-scale measurements. Equipment used to measure and record the field data was somewhat prone to zero drift with the extreme range of temperatures experienced at the test site (±30°C). The field test equipment has since been modified to provide transducer zero readings and recorder calibrations prior to each data run. Corrections for this drift could not be accurately determined and any resulting errors are directly reflected by Fig. 8. With the exception of Run No. 310, the addition of a fixed value for a given full-scale run would improve the agreement between the two sets of coefficients.

TABLE 2

Mean pressure coefficients (C_p)

Run No.	Direction (degrees)	Pressure tap number											
		1	2	3	4	5	6	7	8	9	10	11	12
207	186	0.38	0.43	0.59	0.45	0.64	0.44	0.29	0.32	0.56	0.08		−0.20
21	186	0.49	0.59	−0.76	0.68	0.62	0.22	0.24	0.06	0.14	0.45	−0.21	
310	217	0.26	0.23	−0.18	0.18	−0.38	0.05	−0.05	−0.41		0.22		0.24
23	211	−0.09	−0.11	−0.14	−0.13	−0.18	−0.05	−0.03	−0.04	−0.04	0.08	0.07	
24	211	−1.00	−0.60	−0.53	−0.55	−0.63	−0.22	−0.12	−0.16	−0.02	0.67	−0.19	
311	256	−0.12	0.12	−0.36	−0.45	−0.61	−0.84	−0.21	−0.70		0.46		0.35
22	256	0.10	−0.11	−0.36	−0.55	−0.59	−0.41	0.10	−0.54	−0.18	0.30	0.37	
322	309	−0.52	−0.05	−0.22	−0.20	−0.24	−0.78	−0.47	−0.47		−0.09		0.15
11	341	−0.32	−0.14	−0.15	−0.23	−0.12	−0.50	−0.14	−0.37	−0.10	−0.12	0.30	

TABLE 3

Fluctuating pressure coefficients (C_{pf})

Run No.	Direction (degrees)	Pressure tap number											
		1	2	3	4	5	6	7	8	9	10	11	12
207	186	0.24	0.28	0.32	0.32	0.31	0.21	0.19	0.18	0.21	0.27		0.19
21	186	0.25	0.28	0.31	0.33	0.38	0.08	0.09	0.10	0.08	0.26	0.08	
310	217	0.38	0.33	0.28	0.28	0.32	0.32	0.25	0.22		0.29		0.29
23	211	0.14	0.15	0.15	0.15	0.17	0.09	0.07	0.07	0.04	0.14	0.11	
24	211	0.22	0.10	0.09	0.09	0.10	0.09	0.05	0.07	0.03	0.16	0.07	
311	256	0.70	0.29	0.32	0.40	0.43	0.62	0.31	0.30		0.44		0.43
22	256	0.12	0.19	0.18	0.25	0.20	0.18	0.09	0.24	0.05	0.13	0.16	
322	309	0.30	0.15	0.15	0.17	0.19	0.34	0.21	0.18		0.15		0.18
11	341	0.13	0.05	0.05	0.07	0.07	0.19	0.10	0.11	0.05	0.04	0.12	
101	347	0.31	0.10	0.24	0.12	0.09	0.38	0.25	0.20	0.10	0.25		0.49

TABLE 4

Peak factors (g)

Run No.	Direction (degrees)	Pressure tap number											
		1	2	3	4	5	6	7	8	9	10	11	12
207	186	5.9	6.8	4.4	5.1	4.5	3.7	2.6	3.1	1.5	4.7		3.7
21	186	5.2	7.0	4.5	6.0	4.1	3.8	3.9	6.9	6.8	4.3	4.5	
310	217	4.5	4.9	6.6	7.1	6.4	5.4	3.8	4.3		5.8		4.6
23	211	4.0	6.5	5.7	5.8	5.1	5.3	4.3	4.9	3.9	6.6	3.3	
24	211	2.9	6.2	4.9	5.7	4.3	3.4	3.7	3.5	4.2	5.9	3.1	
311	256	4.9	5.5	5.0	5.0	3.9	4.3	4.8	3.4		5.0		4.7
22	256	5.7	5.4	3.9	7.0	6.3	4.5	4.3	3.3	3.4	3.5	3.9	
322	309	4.2	3.8	5.0	3.7	7.3	4.7	6.5	3.7		3.1		3.1
11	341	3.6	4.4	3.6	4.2	6.6	5.0	3.7	6.3	3.5	4.2	3.6	
101	347	6.4	2.7	2.3	2.8	2.6	4.8	6.4	2.9		2.4		2.0

TABLE 5

Zero crossing rates (Crossings/s)

Run No.	Direction (degrees)	Pressure tap number											
		1	2	3	4	5	6	7	8	9	10	11	12
207	186	0.37	0.34	0.34	0.35	0.36	0.36	0.37	0.39	0.31	0.37		0.25
21	186	0.39	0.43	0.31	0.35	0.33	0.30	0.36	0.34	0.15	0.21	0.26	
310	217	0.23	0.26	0.32	0.31	0.32	0.29	0.27	0.31		0.31		0.11
23	211	0.29	0.33	0.29	0.32	0.35	0.29	0.31	0.34	0.16	0.21	0.16	
24	211	0.47	0.32	0.30	0.33	0.28	0.48	0.45	0.52	0.17	0.33	0.31	
311	256	0.20	0.28	0.26	0.21	0.21	0.24	0.34	0.20		0.26		0.17
22	256	0.30	0.33	0.33	0.36	0.28	0.24	0.29	0.20	0.12	0.19	0.18	
322	309	0.40	0.47	0.45	0.36	0.37	0.32	0.41	0.30		0.31		0.21
11	341	0.34	0.49	0.32	0.35	0.35	0.25	0.27	0.23	0.11	0.22	0.25	
101	347	0.47	0.46	0.48	0.34	0.42	0.33	0.38	0.47	0.44	0.26		0.22

Changes in equipment sensitivity due to temperature variations were found to be small and, therefore, greater confidence can be put in the measurements of pressure fluctuations. Fluctuating pressure coefficients, C_{pf}, plotted in Fig. 9, indicate a fairly good correlation between model and full-scale, the former averaging approximately one-half of the latter. This discrepancy is believed to be due primarily to the low turbulence intensities observed in the model studies, although scale effects cannot be completely ruled out. There is no obvious explanation for the good agreement between Run Nos. 207 and 21, and the relatively poor agreement between Run Nos. 311 and 22. It may be that the pressure fluctuations are quite sensitive to wind direction and that directions were not properly matched in the model studies.

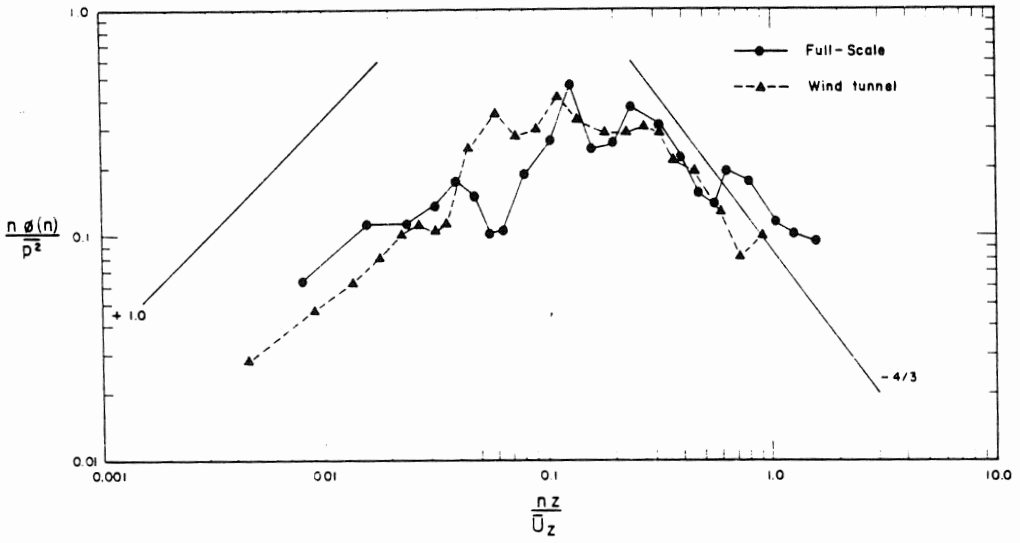

Fig. 10. Pressure spectra (P3, Run Nos. 311 and 22).

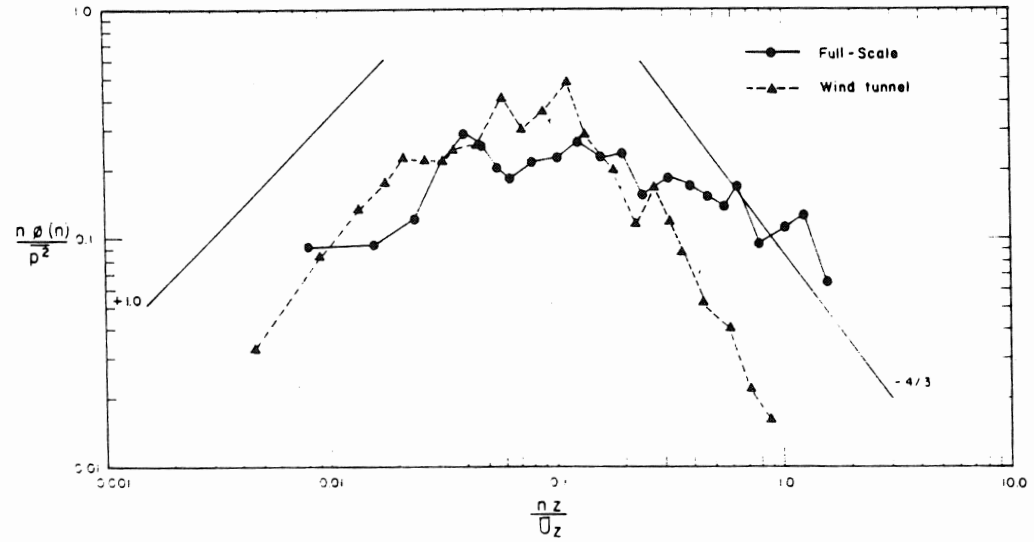

Fig. 11. Pressure spectra (P10, Run Nos. 311 and 22).

It is expected that a new series of tunnel tests in which the turbulence characteristics are more accurately simulated will bring the results into much better agreement

Spectral densities for tap positions P3 and P10 (Run Nos. 311 and 22) are compared in Figs. 10 and 11, respectively. The shapes of the spectra compare quite favorably and suggest a slope of $-4/3$ over the higher frequency range. As indicated previously, the wind data were normalized on the assumption that the scale ratio was 1:50. Although the peaks are not well defined, they suggest a scale ratio in line with that obtained by comparing the velocity spectra.

Spectral densities for the full-scale pressure fluctuations above the spectral peak usually exceeded those obtained from the wind tunnel model (see Fig. 11). This is quite likely due to the fact that the analog filters used in the full-scale studies had a cutoff frequency of 10 Hz, resulting in aliasing errors in the spectral analysis. The wind tunnel pressure signals, on the other hand, were subjected to pronounced attenuation above 100 Hz which would appear as a 2 Hz cutoff in the analysis. Thus the aliasing errors can be expected to be considerably smaller for the wind tunnel data.

Another indication of similarity between model and full-scale pressure fluctuations is the coherence function. The coherence function, or more properly $(\text{coherence})^{1/2}$, is the normalized modulus of the cross-spectrum and is a measure of the correlation between fluctuations at two points over the frequency range for a given separation distance. This function for P1—P6 and Run Nos. 310 and 23 is plotted in Fig. 12.

The peak factors, which are listed in Table 4, are fairly consistent and suggest an average value of 4.6. It has been shown, both theoretically and experimentally [5,6], that the peak factor increases with length of record and

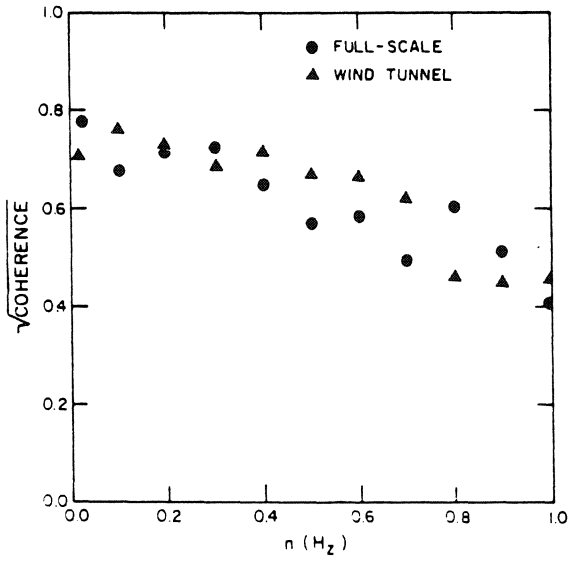

Fig. 12. Coherence (P1—P6, Run Nos. 310 and 23).

TABLE 6

Area-averaged coefficients

Run No.	Direction (degrees)	Tap combination	C_{pf}	g	Area (m^2)			
310	217	1,2,3	0.28	4.6	(0.76)	(4.27)	=	3.25
310	217	1,2,3,10	0.40	6.2	(0.76)	(4.27)	=	3.25
310	217	1,2,3,6,7,10,12	0.21	4.3	(5.61)	(4.27)	=	23.97
322	309	1,2,3	0.12	4.3	(0.76)	(4.27)	=	3.25
322	309	1,6	0.27	5.3	(0.82)	(5.61)	=	4.65
322	309	4,5,10	0.12	8.8	(0.76)	(3.05)	=	2.32

a value of $g = 4.3$ has been suggested for calculating design loads on cladding elements for those situations where resonant response is insignificant. The peak factors in Table 4 are based upon single records of 750 seconds and represent a worst-case excursion from the mean, *i.e.* negative excursions for pressure taps 1—9 and positive excursions for taps 10—12. It should be pointed out that the peak factors will vary from record to record for a given wind speed and direction and that several records would be required to establish their mean and variance.

Fluctuating pressure coefficients and peak factors determined from the area-integration of pressure records are presented in Table 6. The procedure was to construct a new pressure-time series by multiplying the samples of each record to be summed by a weighting factor. The weighting factor was proportional to the area attributed to each pressure tap which implies that all pressure fluctuations over that area are perfectly correlated. The resulting record was then analyzed in the usual manner. As expected, the fluctuating pressure coefficients show a decrease with increasing area, but there is no indication of a similar reduction in the peak factor. Although the transducer separations used in this study do not permit a detailed assessment of the correlation of peak pressures acting over extended roof areas, some indication of the area reduction of peak pressures can be derived from Table 6. Comparing the product of the fluctuating pressure coefficient and peak factor for transducer combinations 1, 2, 3 for Run No. 332 with the product of the averaged fluctuating pressure coefficients and peak factors for the individual transducers (Tables 3 and 4), the corresponding reductions in peak pressure fluctuations are approximately 27 and 40%, respectively. A similar comparison for the combination 1, 2, 3, 6, 7, 10, 12 (Run No. 310) indicates a reduction of 42%. In averaging the pressure records, it was assumed that the pressure fluctuations under the eaves overhang were perfectly correlated and equal to the fluctuations measured by transducer No. 10. An increase of 42% was obtained from the combination 1, 2, 3, 10 for Run No. 310. It should be noted that the records for transducer Nos. 10 and 12 were inverted so that positive fluctuations acted in the same sense as negative fluctuations on the roof.

7. Comparison with recommended design loads

In addition to providing a check on wind tunnel test results, the full-scale data reported herein allow some direct comparisons with current recommended design wind loads. American National Standard Building Code Requirements for Minimum Design Loads in Buildings and Other Structures, A58.1—1972, states a procedure for calculating wind loads on roofs and considers both tributary (parts and portions) and total roof areas [7]. The basic wind speeds used in this document are the fastest-mile speeds for a 50-year mean recurrence interval and flat, open country (Exposure C) at a height of 30 ft above the ground.

Because they are defined differently, the pressure coefficients measured in full scale and those specified in the A58.1 Standard cannot be compared directly. However, the pressures can be compared for a given wind speed and category of exposure. Assuming flat, open country and a basic wind speed of 40.2 m/s, the corresponding effective velocity pressures for heights less than 10 m are as follows:

q_f = 960 N/m^2 (A58.1 — Table 5 — Ordinary buildings and structures)
q_p = 1480 N/m^2 (A58.1 — Table 6 — Parts and portions)

For buildings with a ratio of wall height to least width of less than 2.5, the A58.1 Standard specifies a general external pressure coefficient of −0.7 for roofs. For gabled roofs with the wind direction perpendicular to the ridge and the height-width ratio and roof slope being considered here, a pressure coefficient of −1.0 is specified for the windward slope. The Standard also allows for local peak pressures which are assumed to act at 90° corners and on strips running along the ridge and eaves. The width of these strips is taken as 10% of the least width of the building normal to the ridge. The specified pressure coefficients are −2.4 for ridges and eaves and −3.9 for 90° corners.

No specific provision is made for pressures on the underside of eaves, but this can be taken as the pressure acting on the windward wall for which a coefficient of 0.8 is specified. Internal pressures are based on the fastest-mile speed at 30 ft. above ground for the appropriate terrain category and an internal pressure coefficient, C_{pi}, which is related to the distribution of wall openings and the ratio of open to solid wall area. The design pressures for the assumed wind speed and exposure are as follows:

(a)	Leeward slope, total area	=	(−0.7)	(960)	= −670 N/m^2
(b)	Windward slope, total area	=	(−1.0)	(960)	= −960
(c)	Leeward slope, tributary area	=	(−0.7)	(1480)	= −1040
(d)	Windward slope, tributary area	=	(−1.0)	(1480)	= −1480
(e)	Ridges and eaves	=	(−2.4)	(1480)	= −3550
(f)	90-degree corners	=	(−3.9)	(1480)	= −5780
(g)	Underside of eaves	=	(0.8)	(1480)	= 1190
(h)	Internal pressure	=	(0.3)	(1000)	= 300

At Z = 10 m, the corresponding mean speed averaged over 750 seconds (the record length used in this study) is approximately 33.5 m/s (see ref. [8]). For standard atmospheric conditions the effective velocity pressure is 670 N/m^2 Using the full-scale pressure coefficients listed in Tables 2, 3 and 4, the mean and peak pressures were calculated for 10 transducer locations and four wind directions. The results are presented in Fig. 13 along with the design pressures specified by the A58.1 Standard (case (f) excepted).

It is seen from Fig. 13 that the negative design pressures for the total leeward and windward roof areas (lines (a) and (b)) exceed the observed mean pressures for all transducer locations. However, the observed peak pressures dominate and exceed the design pressures for tributary areas (lines (c) and (d)) at several locations. This may or may not be significant, depending on the degree to which pressure fluctuations are correlated over the roof area. The design pressures for ridges and eaves (line (e)) substantially exceed the observed peak pressures and the design pressure for 90° corners is approximately 2.5 times the maximum observed negative pressure. The positive design pressure for the underside of the eaves (line (g)) is exceeded by the observed peak pressure for two wind directions and the internal design pressure (line (h)) is less than the measured peak internal pressure for all four wind directions.

As discussed previously, the fluctuating pressure coefficients determined from the area-integration of pressure records decrease with increasing area while the peak factors remain about the same. Although reductions of from 20 to 40% in the peak pressures (peak departures from the mean) are indicated

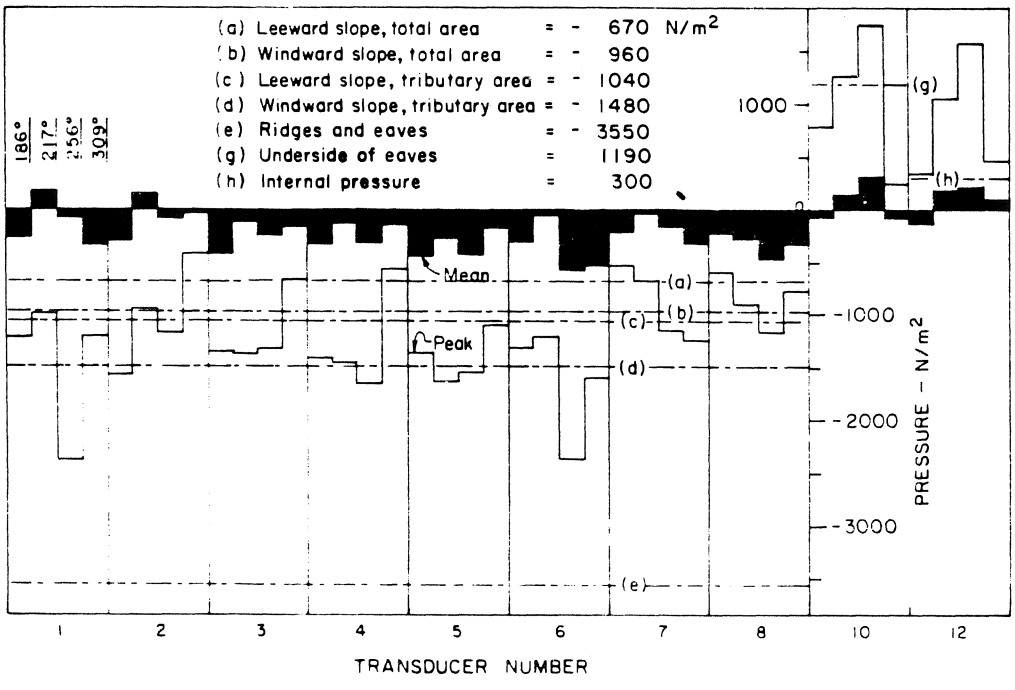

Fig. 13. Comparison of measured and specified design pressures.

for roof areas of up to 5 m^2, the data presented in Fig. 13 suggest that the provisions of the A58.1 Standard for tributary roof areas are marginal.

The provisions for ridges and eaves and for 90° corners, on the other hand, appear to be overly conservative. The maximum negative pressure, based on the measured coefficients, was -2390 N/m^2 for transducer No. 1 at 256° while the design pressures are -3550 N/m^2 for ridges and eaves and -5780 N/m^2 for 90° corners. It is recognized that extreme negative pressures are associated with vortices generated along the edges of the roof and that these vortices are extremely sensitive to wind direction and roof geometry. However, the wind tunnel studies described previously did not reveal any critical wind directions not covered by the full-scale data. If the effective velocity pressure of 960 N/m^2 (q_f) is used in place of 1480 N/m^2 (q_p), the resulting design pressures are -2300 N/m^2 for ridges and eaves and -3730 N/m^2 for 90° corners.

As with the negative pressures acting over the roof area, the peak pressures under the eaves (transducer No. 10) and in the garage area (transducer No. 12) far exceed the corresponding mean pressures averaged over the record length of 750 seconds. Again referring to Table 6 and Fig. 13, the average maximum pressure (peak plus mean) acting upward on the eaves is 1680 N/m^2 for Run No. 310 and combination 1, 2, 3, 10. The corresponding design uplift pressure is 3540 + 1200 = 4740 N/m^2. For combination 1, 2, 3, 6, 7, 10, the average maximum pressure acting over a roof area of 24 m^2 is 140 + 620 = 760 N/m^2 as compared with 1040 + 300 = 1340 N/m^2 (tributary area plus internal pressure) as specified by the A58.1 Standard.

The maximum internal pressure (based on measured coefficients) in the garage area was approximately five times the corresponding design pressure. The ratio of effective open area to solid area is difficult to determine since all doors and windows were closed during the recording intervals reported herein. One door and one window of approximately 1.8 and 1.4 m^2, respectively, are located on the S.E. wall, one window of 1.4 m^2 on the S.W. wall, and an overhead garage door of 5.1 m^2 is situated on the N.W. wall. Because of the extremely cold winters in Montana, great care is usually taken to provide doors and windows with adequate seals or weatherstripping. It is probable, therefore, that infiltration rates for this garage area would compare with those for living quarters in regions having a mild climate.

8. A procedure for the calculation of design pressures

The 1970 edition of the National Building Code of Canada (NBC) [9] provides for risk of occurrence, terrain roughness, height above ground and building geometry in calculating design wind pressures

$$p = q\, C_e\, C_g\, C_p \qquad (1)$$

In this expression, q is a reference mean velocity pressure for a given mean recurrence interval, C_e is an exposure factor which varies with surface roughness and height above ground, C_g is a gust effect factor to provide for the

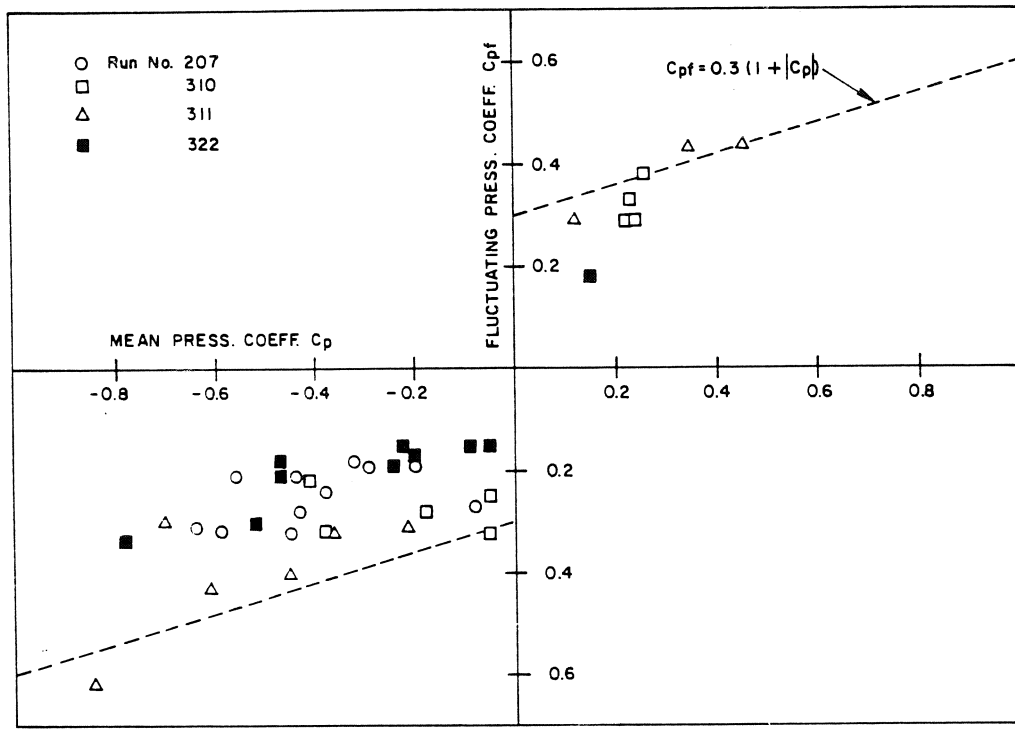

Fig. 14. C_p *versus* C_{pf} — full scale.

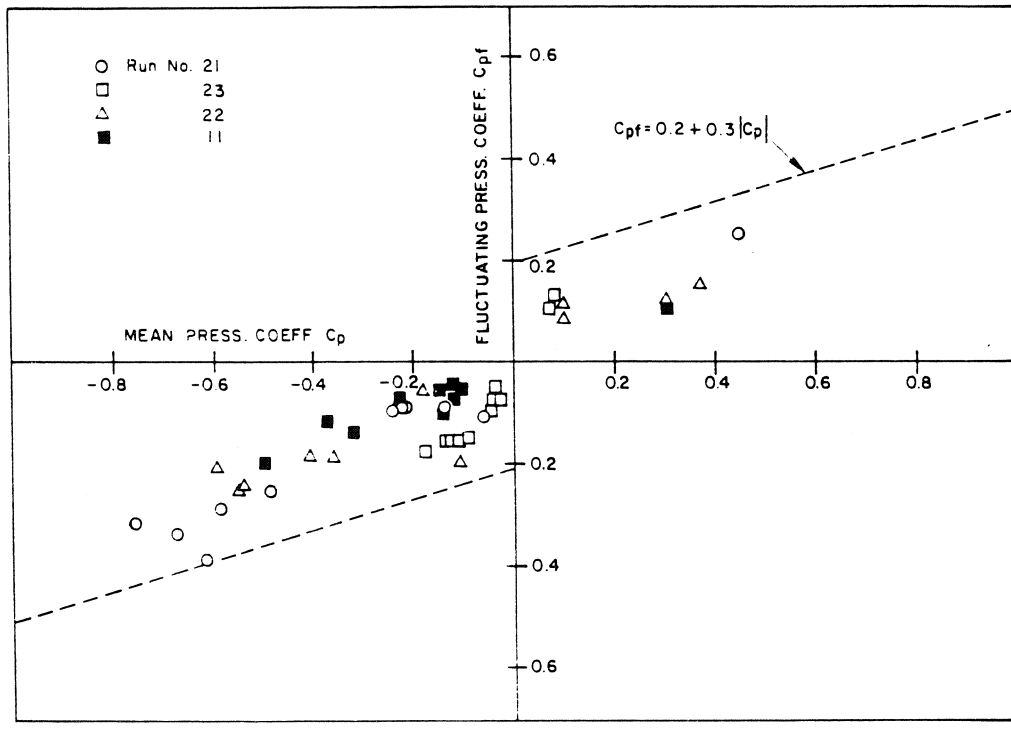

Fig. 15. C_p *versus* C_{pf} — wind tunnel.

dynamic response characteristics of the structure and surface pressure fluctuations caused by turbulence and localized flow phenomena, and C_p is the conventional mean pressure coefficient determined from wind tunnel tests. For the design of cladding, it is assumed that dynamic response can be neglected and a factor of 2.5 is used for C_g.

The form of eqn. (1) is particularly convenient in that it allows a complex process to be treated as a combination of independent elements and provides for the separate treatment of mean and fluctuating components of pressure. The peak design pressure at any point on a roof area can be expressed as

$$p = C_g \bar{p} = \bar{p} \pm g p_{\text{r.m.s.}}$$

Or, in terms of dimensionless pressure coefficients based upon a suitable reference pressure, such as the free-stream dynamic pressure at $Z = 10$ m

$$C_g = 1 + g \frac{C_{pf}}{|C_p|} \tag{2}$$

While eqn. (2) is a practical means of expressing C_g, full-scale and wind tunnel measurements (Figs. 14 and 15) suggest an empirical relationship between C_{pf} and C_p. If the envelope of full-scale C_{pf} values is expressed as:

$$C_{pf} = 0.3(1 + |C_p|)$$

and it is assumed that $g = 5.0$, eqn. (2) becomes

$$C_g = 1 + 1.5 \frac{(1 + |C_p|)}{|C_p|} \tag{3}$$

As indicated earlier, the peak factor g does not appear to change with surface area. Therefore, it may be possible to determine a gust effect factor, C_g^a, for extended roof areas simply by reducing C_{pf} by means of a factor, R_p, roughly analogous to the size reduction factor used in calculating dynamic response. The gust effect factor would then be defined by:

$$C_g^a = 1 + 1.5 \frac{(1 + |C_p|)R_p}{|C_p^a|} \tag{4}$$

where C_p^a is the corresponding mean pressure coefficient for the extended roof area.

9. Conclusions

The use of spires at the entrance of a wind tunnel working section substantially increases the growth rate of rough wall boundary layers, thereby placing the study of building aerodynamics within the capability of many conventional tunnels. However, the use of spires and scaled upwind roughness elements does not alone ensure the establishment of flows with proper turbulence characteristics. A minimum degree of surface roughness is required to

establish suitable scales and intensities of turbulence. With some modification of the roughness elements, it is believed that close simulation of the lowest 30 m of the atmospheric boundary layer can be achieved at a scale ratio of 1:50.

The agreement between model and full-scale spectra for both velocity and pressure fluctuations is encouraging. Measurements of coherence suggest that the spatial extent of surface pressure fluctuations can be modeled to an acceptable degree of accuracy.

It is believed that the consistently low values of C_{pf} determined from the model result primarily from improper simulation of the turbulence. However, scale effects cannot be ruled out at this time. Peak factors were found to agree quite closely with previous measurements, the overall average for model and full-scale results being 4.6. Based on the preliminary results reported herein, it appears that a gust effect factor can be expressed in terms of a peak factor, mean pressure coefficients and a size reduction factor.

Wind pressures based on measured coefficients and an assumed wind speed suggest that certain provisions of the current A58.1 Standard deserve additional study. For the building investigated, design pressures for tributary areas and interiors appear to be marginal while those for localized areas such as ridges, eaves and corners appear to be excessive.

10. Acknowledgements

Acknowledgement is made to the Tri Service Building Materials Investigational Program Committee, Department of Defense, for financial support of the field studies reported herein. The writer wishes to express his thanks to Lt. Col. C.Y. Holland, Jr., USAF, for his assistance at the field test site and to Col. R.A. Nelson and Family whose home was instrumented during the course of the study. Special thanks are extended to Dr. H.I. Laursen who developed much of the computer software used in the data analysis during his term as a Visiting Researcher at the NBS.

Nomenclature

C_{dp}	dynamic pressure correction coefficient
C_e	exposure factor
C_g	gust effect factor
C_p	mean pressure coefficient
C_{pf}	fluctuating pressure coefficient
C_{sp}	static pressure correction coefficient
I	intensity of turbulence, (%)
$\bar{U}_{10}$	mean velocity at standard 10-m height,(m/s)
$\bar{U}_R$	reference mean velocity at 6.6 m
Z	height above ground, (m)
Z_G	gradient height

Z_o	surface roughness height, (cm)
g	peak factor
$\bar{p}$	mean pressure, (N/m^2)
$p_{r.m.s.}$	r.m.s. pressure
$\bar{p}_R$	reference dynamic pressure at 6.6 m
$\bar{p}_{10}$	reference dynamic pressure at 10 m
q	reference dynamic pressure for open country
R_p	size reduction factor
β	wind direction measured clockwise from north, (degrees)
ρ	mass density of air
ϕ	spectral density

References

1 W.H. Melbourne, Comparison of pressure measurements made on a large isolated building in full and model scale, Proc. Third Int. Conf. on Wind Effects on Buildings and Structures, Tokyo, 1971, pp. 253—262.

2 N.M. Standen, A spire array for generating thick turbulent shear layers for natural wind simulation in wind tunnels, Nat. Aeronaut. Establishment Rep. LTR—LA—94, Ottawa, May 1972.

3 R.D. Marshall and G. Hsi, Techniques for measuring wind loads on full-scale buildings, Proc. Research Seminar on Wind Loads on Structures, Univ. of Hawaii, October 1970, pp. 133—148.

4 N.C. Helliwell, Wind over London, Proc. Third Int. Conf. on Wind Effects on Buildings and Structures, Tokyo, 1971, pp. 23—32.

5 W.A. Dalgliesh, Statistical treatment of peak gusts on cladding, Proc. of the Structural Division, ASCE, Sept. 1971, pp. 2173—2187.

6 A.G. Davenport, Note on the distribution of the largest value of a random function with application to gust loading, Paper No. 6739, Proc. Inst. Civil Eng., 28 (1964) 187—196.

7 American National Standard Building Code Requirements for Minimum Design Loads in Buildings and Other Structures, A58.1—1972, issued by American Nat. Stand. Inst., New York.

8 E.L. Deacon, Wind gust speed; averaging time relationships, Aust. Meteorol. Mag., 51 (1965) 11—14.

9 National Building Code of Canada 1970, issued by the Assoc. Comm. on the NBC, National Research Council, Ottawa, Canada.